ACS Sustainable Chemistry & Engineering

Research Article

Cite This: ACS Sustainable Chem. Eng. 2019, 7, 15706−15714

pubs.acs.org/journal/ascecg

Engineering an Alcohol Dehydrogenase for Balancing Kinetics in NADPH Regeneration with 1,4-Butanediol as a Cosubstrate

Guochao Xu,[†,#] Cheng Zhu,[†,#] Aitao Li,[‡] Yan Ni,[§] Ruizhi Han,[†] Jieyu Zhou,[†] and Ye Ni*[,†]

[†]Key Laboratory of Industrial Biotechnology, Ministry of Education, School of Biotechnology, Jiangnan University, Wuxi 214122, Jiangsu, China

[‡]Hubei Collaborative Innovation Center for Green Transformation of Bio-resources, Hubei Key Laboratory of Industrial Biotechnology, College of Life Sciences, Hubei University, Wuhan 430062, China

[§]Department of Biomedical Engineering, Eindhoven University of Technology, NL-5600 Eindhoven, MB, Netherlands

Supporting Information

ABSTRACT: Cofactor regeneration using diols as "smart cosubstrates" is one of the most promising approaches, due to the thermodynamic preference and 0.5-equiv requirement. In order to establish an efficient NADPH regeneration system with 1,4-butanediol (1,4-BD), a $NADP^+$-dependent alcohol dehydrogenase from *Kluyveromyces polysporus* (*Kp*ADH) was engineered to solve the kinetic imbalance. Several hotspots were identified through molecular dynamic simulation and subjected to saturation and combinatorial mutagenesis. Variant $KpADH_{V84I/Y127M}$ exhibited a lower K_M of 15.1 mM and a higher k_{cat} of 30.1 min^{-1} than $^{WT}KpADH$. The oxidation of 1,4-BD to 4-hydroxybutanal was found to be the rate-limiting step, for which the k_{cat}/K_M value of double mutant $KpADH_{V84I/Y127M}$ was 2.00 $min^{-1}{\cdot}mM^{-1}$, 11.6-fold higher than that of $^{WT}KpADH$. $KpADH_{V84I/Y127M}$ preferred diols with a longer chain length (C5−C6). The ratio of k_{cat}/K_M toward 2-hydroxytetrahydrofuran (2-HTHF), in comparison to 1,4-BD, in $KpADH_{V84I/Y127M}$ was dramatically reduced by almost 100-fold compared to $^{WT}KpADH$, which was advantageous for NADPH regeneration. As much as 100 mM phenylpyruvic acid could be reduced into D-phenylalanine with 99.2% conversion in 6 h using merely 0.5 equiv of 1,4-BD. Both the improved catalytic efficiency toward 1,4-BD and the balanced k_{cat}/K_M between 1,4-BD and 2-HTHF contributed to the higher NADPH regeneration efficiency. This study provides guidance for engineering alcohol dehydrogenases for cosubstrate specificity toward diols and its application in NADPH regeneration for the preparation of chiral compounds of pharmaceutical relevance.

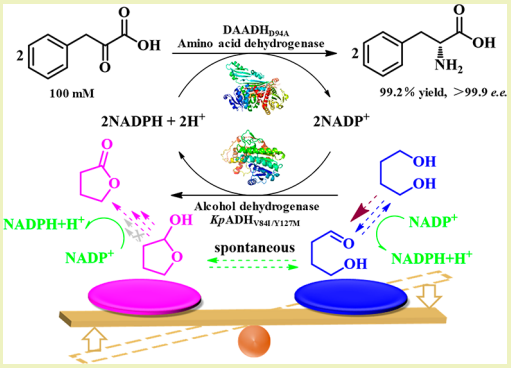

KEYWORDS: *NADPH, Smart cosubstrate, 1,4-butanediol, Cofactor regeneration, Balancing kinetics*

INTRODUCTION

The application of biocatalysis in the preparation of chiral compounds has undergone a revolution over the past few decades from "state of the art" to "the first choice for chemists". The desirability of biocatalysts stems from their outstanding characteristics, such as high enantioselectivity, renewability, and biodegradability, qualities especially attractive to the burgeoning field of green chemistry.[1−3] This is particularly true for redox reactions, including alcohol or amino acid dehydrogenases used in the reduction of the C═O bond, ene or enoate reductases used for reduction of the C = C bond, and oxygenases for oxyfunctionalization.[4−6] The chiral compounds produced are of high economic value and are used widely as food ingredients and building blocks for the production of pharmaceuticals.[7,8] Most of the reactions mentioned above, however, require stoichiometric amounts of NAD(P)H, which can be very expensive.[9] As an economic and practical approach, NAD(P)H should be added in catalytic amounts and regenerated in situ.[10]

Intensive research has been committed to the development of efficient NAD(P)H regeneration systems, which have been accomplished by enzyme-coupled, substrate-coupled, electroenzymatic, photochemical, and chemical approaches.[11−14] For a practical cofactor regeneration approach, the cosubstrates should be inexpensive, the reactions should be thermodynamically and kinetically favorable, and the coproducts should be separable and noninhibitory.[15] Considering all these factors, well-established enzyme- and substrate-coupled approaches are currently more attractive for regeneration of nicotinamide cofactors.[8] Alcohol dehydrogenase (ADH)-catalyzed oxidation of simple alcohols (such as ethanol and isopropanol) represents the most elegant example of this approach (Table 1). Ethanol is a four-electron reductant, and it is especially attractive as a cosubstrate due to its favorable redox potential

Received: July 7, 2019
Revised: August 17, 2019
Published: August 19, 2019

DOI: 10.1021/acssuschemeng.9b03879
ACS Sustainable Chem. Eng. 2019, 7, 15706−15714

Table 1. Comparison of the Thermodynamic, Substrate Price, and Waste Amount of Various NADPH Regeneration Approaches

cosubstrate	coproduct	catalyst	price [$·mol^{-1}]	$\Delta G'$ rxn [kcal·mol^{-1}][a]	waste [g·mol^{-1}·prod.]
HCO_2H	CO_2	FDH	1.11	−4.6	44
isopropanol	acetone	ADH	1.29	−6.1	58
ethanol	acetic acid	ADH/AldDH	0.55	−7.4	30
H_3PO_3	H_3PO_4	PDH	3.04	−15	98
glucose	gluconic acid	GDH	1.21	−6.9	196
1,4-BD	GBL	*Kp*ADH	1.03	−8.2	43

[a]$\Delta G'$ rxn of each cosubstrate was cited and calculated according to ref 16; the price of each cosubstrate was cited from commercial source.

($\Delta G'$ of −7.4 kcal·mol^{-1}), economic price (0.55 $·mol^{-1}), availability, and dual function as a cosolvent and cosubstrate.[16] However, this bienzymatic approach depends on both ADH and aldehyde dehydrogenase, and acetic acid as the coproduct can cause a drop in reaction pH, which requires additional pH control. Isopropanol is another commonly used cosubstrate with high efficiency in the regeneration of NADH or NADPH.[8] However, isopropanol must be applied in significant molar excess, and the acetone produced needs to be removed to drive the reaction forward and prevent enzyme inactivation.[17] Consequently, there remains a constant demand for new and improved cofactor regeneration approaches.

A simple approach has been developed by Hollmann et al. by employing lactonizable diols as "smart cosubstrates".[18] The preliminary step involves 1,4-butanediol (1,4-BD) reduced into 4-hydroxybutanal (step 1) and then spontaneously converted into 2-hydroxytetrahydrofuran (2-HTHF) (Scheme 1). The

Scheme 1. Reaction Path for the Enzymatic Oxidation of Diols

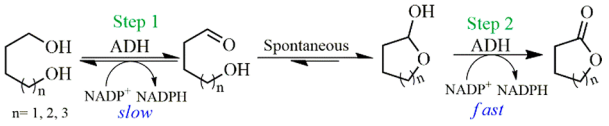

second step is an irreversible reduction into γ-butyrolactone (GBL) (step 2), with a $\Delta G'$ of −8.2 kcal·mol^{-1}, which liberates 2 equiv of NAD(P)H. In addition, the final product, GBL, can be considered an important bulk chemical and is thermodynamically stable and kinetically inert. This quality could shift the equilibrium and thereby reduce the molar excess requirement of the cosubstrate.[19] This novel regeneration approach has been applied to NADH regeneration by employing HLADH, *Te*SADH, or evo 1.1.200.[19−25] However, NADPH regeneration approaches have so far been insufficiently developed, and only a few ADHs capable of regenerating NADPH using diols have been reported. ADH from *Lactobacillus brevis* (*Lb*ADH) has been shown to be able to catalyze the oxidation of 1,4-BD and 1,6-hexanediol (1,6-HD), but the low activity of the enzyme and inhibition at 197 mM diols makes this system less than ideal.[22] Considering many industrial enzymes are NADPH-dependent, engineering ADHs for regenerating NADPH by oxidation of diols is of particular interest.

An NADPH-dependent alcohol dehydrogenase (*Kp*ADH) was identified from *Kluyveromyces polysporus* by genome mining and was demonstrated to be capable of reducing bulky−bulky ketones with moderate enantioselectivity.[26] *Kp*ADH has been shown to follow the ordered Bi−Bi kinetic mechanism and "Prelog" priority in the reduction of prochiral ketones.[27] Employing hydroclassified combinatorial saturation mutagenesis (HCSM) and polarity scanning strategies, the *e.e.* values of *Kp*ADH were increased to 99.4% (*R*) and reversed to 97.8% (*S*) in the reduction of 500 mM (4-chlorophenyl)-(pyridine-2-yl)ketone.[28,29] Unlike homologous enzymes, such as Gre2p (51.3%) and CgKR1 (50.4%), *Kp*ADH exhibits high oxidative activity toward secondary alcohols such as isopropanol but has relatively lower activity toward 1,4-BD. Moreover, the analysis of kinetic constants revealed that the oxidation of 1,4-BD is the rate-limiting step, and there is a remarkable difference in kinetics between step 1 and step 2. Our strategy for the regeneration of NADPH with diols as "smart cosubstrates" was then focused on improving the efficiency of *Kp*ADH toward 1,4-BD and balancing the kinetics between the two steps. The feasibility of this newly developed NADPH regeneration enzyme was evaluated in the preparation of D-amino acids.

EXPERIMENTAL SECTION

General Remarks. 1,4-Butanediol (1,4-BD), 1,5-pentanediol (1,5-PD), and 1,6-hexanediol (1,6-HD) were purchased from Aladdin (Shanghai) Co., Ltd. $NADP^+$ and NADPH were bought from Bontac Bio-engineering (Shenzhen) Co., Ltd. PPA was purchased from Bodi Biotechnology (Shanghai) Co., Ltd. D-Phe was purchased from CIVI Chemical Technology (Shanghai) Co., Ltd. Other reagents were purchased from Sinopharm (Shanghai) Co., Ltd. unless otherwise stated.

Construction of Mutant Library and High Throughput Screening. Saturation mutagenesis library was constructed employing whole plasmid PCR with recombinant pET28-*kpadh* coding for the alcohol dehydrogenase *Kp*ADH as a template. PCR amplification system was as follows: 1.8 μL of dNTP mixture, 0.2 μL of PrimeSTAR HS DNA polymerase, 4 μL of 5× PrimeSTAR HS DNA polymerase buffer, 0.4 μL of forward primer, 0.4 μL of reverse primer (Table S1), 0.4 μL of pET28-*kpadh*, and 12.4 μL of ddH_2O. The PCR program was predenaturation at 94 °C for 4 min, followed by amplification for 20 cycles with denaturation at 98 °C for 10 s, annealing at 55 °C for 15 s and elongation at 72 °C for 6 min, and then further elongation at 72 °C for 10 min. The resultant PCR product was digested with *Dpn*I at 37 °C for 0.5 h to eliminate the parental plasmid. Then, 10 μL of the digestion mixture was transformed into *Escherichia coli* BL(DE3). Single colonies were picked up and inoculated into 300 μL of LB medium (50 μg·mL^{-1} Kan) in each well of a 96-deep well plate and further incubated at 37 °C for 12 h. Furthermore, 50 μL culture was transferred into another 96-deep well plate containing 600 μL of LB in each well (50 μg·mL^{-1} of Kan). After incubation at 37 °C and 120 rpm for 2.5 h, 0.2 mM IPTG was added and further cultivated at 25 °C and 120 rpm for 5 h. Cells were harvested by centrifugation at 4000 rpm for 10 min and stored at −80 °C. Then cells thawed and were treated with 750 mg·L^{-1} of lysozyme at 37 °C for 1 h. The cell lysate was collected by centrifugation at 4000 rpm for 10 min.

Activity Assay. The oxidative activities were determined by monitoring the increased absorbance of NADPH at 340 nm with a molar extinction coefficient of 6220 L·mol^{-1}·cm^{-1}. The reaction mixture consisted of 10 mM diols, 1 mM $NADP^+$ in glycine-NaOH buffer (pH 9.5, 100 mM), and 10 μL supernatant at 30 °C for 3 min. One unit of oxidative activity was defined as the amount of enzyme required to catalyze the produce of 1 μmol NADPH per minute under the above-mentioned activity assay condition.

Rescreening of Beneficial Mutants. *Kp*ADH variants with higher activity were inoculated into 40 mL of LB medium, cultivated

DOI: 10.1021/acssuschemeng.9b03879
ACS Sustainable Chem. Eng. 2019, 7, 15706−15714

Table 2. Kinetic Parameters of ^{WT}*Kp*ADH and Variants toward $NADP^+$ and 1,4-BD

variant	K_{ia} [μM][a]	$K_{M,NADP^+}$ [μM]	$K_{M,1,4\text{-BD}}$ [mM]	k_{cat} [min^{-1}]	k_{cat}/K_M to 1,4-BD[b] [$min^{-1}\cdot mM^{-1}$]
^{WT}*Kp*ADH	26.7 ± 4.5	15.8 ± 1.8	50.6 ± 6.7	8.76 ± 0.4	0.173 ± 0.015
*Kp*ADH$_{V84I}$	10.7 ± 1.9	30.9 ± 2.2	86.6 ± 8.3	80.3 ± 3.9	0.927 ± 0.044**
*Kp*ADH$_{Y127C}$	757 ± 103	8.34 ± 2.8	21.4 ± 8.6	18.1 ± 0.9	0.846 ± 0.030**
*Kp*ADH$_{Y127M}$	39.7 ± 6.7	14.7 ± 1.5	28.9 ± 4.5	32.4 ± 1.2	1.12 ± 0.133**
*Kp*ADH$_{S196A}$	44.9 ± 2.8	24.7 ± 0.9	45.9 ± 2.6	13.8 ± 0.2	0.301 ± 0.013*
*Kp*ADH$_{F197W}$	347 ± 77	17.2 ± 2.7	12.2 ± 4.5	8.21 ± 0.4	0.673 ± 0.022**
*Kp*ADH$_{V84I/Y127C}$	493 ± 78	9.99 ± 2.5	17.7 ± 5.0	23.0 ± 0.9	1.30 ± 0.152**
*Kp*ADH$_{V84I/Y127M}$	49.7 ± 5.5	3.05 ± 0.7	15.1 ± 1.4	30.1 ± 0.4	2.00 ± 0.158**
*Kp*ADH$_{Y127C/S196A}$	194 ± 13	9.21 ± 1.3	31.0 ± 3.3	28.7 ± 0.7	0.926 ± 0.076**
*Kp*ADH$_{S196A/F197W}$	70.8 ± 5.3	10.0 ± 0.8	23.4 ± 1.8	10.2 ± 0.2	0.436 ± 0.025**

[a] K_{ia} denotes the dissociation constant toward $NADP^+$. [b] k_{cat}/K_M was determined according to k_{cat} and $K_{M,1,4\text{-BD}}$. Statistic analysis was performed: * indicates a statistically significant difference ($p < 0.05$), ** indicates an extremely significant difference ($p < 0.01$).

at 37 °C and 120 rpm. Until OD_{600} reached 0.6−0.8, 0.2 mM IPTG was added and further cultivated at 25 °C and 120 rpm for 6 h. The cells were harvested by centrifugation at 8000 rpm and 4 °C for 10 min, resuspended with phosphate buffer (100 mM, pH 7.0), and disrupted with a nano-homogenizer (AH-BASIC-I, ATS). The activities of variants toward different diols were measured as above-mentioned. Protein concentration was determined by the Bradford method with BSA as the standard protein.

Expression and Protein Purification of *Kp*ADH Variants. To purify the ^{WT}*Kp*ADH and variants, the collected cells were resuspended in 10 mL of buffer A (20 mM imidazole and 500 mM NaCl in 20 mM PBS buffer) and disrupted by ultrasonication (work for 1 s, pause for 3 s, 450 W). Cell debris were removed by centrifugation at 8000 rpm and 4 °C for 30 min. Then, the supernatant was passed through a 0.22 μm filter and loaded on the HisTrap HP nickel affinity column pre-equilibrated with buffer A using an AKTA Avant system (GE Healthcare Co., Ltd.). Target proteins were radiantly eluted employing buffer A and buffer B (500 mM imidazole and 500 mM NaCl in 20 mM PBS buffer). Target proteins were collected and verified by SDS-PAGE analysis. ^{WT}*Kp*ADH and variants were concentrated and mixed with 20% glycerol, and stored at −80 °C for further use (Figure S3−S12).

Determination of Kinetic Parameters. Kinetic parameters of the purified ^{WT}*Kp*ADH and variants were determined employing the standard activity assay method. Different concentrations of 1,4-BD (20.0−250 mM) or 2-HTHF (1.0−25.0 mM), $NADP^+$ (0.01−0.60 mM) and an appropriate amount of purified enzymes were mixed in pH 9.5 glycine-NaOH buffer and 30 °C. All the activities were determined in triplicate. The K_M, V_{max}, k_{cat} and K_{ia} were calculated according to the simulation based on Michaelis−Menten double substrate kinetics employing Matlab software package (Figure S17−S18).

Application of *Kp*ADH$_{V84I/Y127M}$ in NADPH Regeneration with 1,4-BD as a "Smart Cosubstrate". Reaction mixtures for the comparison of different NADPH regeneration systems consisted of 50 mM 1,4-BD or 100 mM glucose, 0.5 mM $NADP^+$, 50 mM PPA, 100 mM ammonium sulfate, 1.5 kU·L^{-1} purified ^{WT}*Kp*ADH, *Kp*ADH$_{V84I}$, *Kp*ADH$_{Y127C}$, *Kp*ADH$_{V84I/Y127C}$ and *Kp*ADH$_{V84I/Y127M}$ or glucose dehydrogenase in 200 mM Gly-NaOH (pH 9.0). Reactions were started by the addition of DAADH$_{D94A}$ partially purified by heating and incubated at 30 °C and 120 rpm. Aliquot samples (100 μL) were withdrawn at intervals, and the reaction was stopped by heating at 100 °C for 10 min, followed by centrifugation at 12000 rpm for 5 min. The formation of D-Phe and γ-butyrolactone was monitored by HPLC and GC.

Studies of the effect of 1,4-BD addition and PPA concentrations on the reaction were conducted with 50 mM or 100 mM PPA, 25 mM or 50 mM 1,4-BD, 100 mM or 200 mM ammonium sulfate, 0.5 mM $NADP^+$, 1.5 kU·L^{-1} purified *Kp*ADH$_{V84I/Y127M}$ in 200 mM Gly-NaOH (pH 9.0). The reactions were also started and monitored as above-described. TOF was defined as one μmol of D-Phe formed in 1 min by using one μmol of *Kp*ADH$_{V84I/Y127M}$ and determined over the first half hour.

Analytical Methods. D-Phe was determined by high-performance liquid chromatography (HPLC) using Astec CHIROBIOTICTM T column (150 mm × 4.6 mm × 5 μm, Sigma Technologies Co. Ltd.) with methanol and ultrapure water (70:30, v/v) as the mobile phase. The retention time of D-Phe was 8.49 min at 210 nm and 30 °C with a flow rate of 0.5 mL·min^{-1} (Figure S15). GBL was measured by gas chromatography (GC) equipped with CP-Chirasil-Dex CB (25 m × 0.25 mm × 0.25 μm, Agilent Technologies Co. Ltd.). The column temperature was initially kept at 70 °C for 5 min and increased to 200 °C at 20 °C·min^{-1} and kept for 5 min. The injector and detector temperatures were 250 °C. The retention time of GBL was 7.92 min (Figure S16).

Molecular Docking and Molecular Dynamic Analysis. Docking runs were carried out using standard parameters of the program for interactive growing and subsequent scoring. Molecular dynamic simulation was carried out employing the NAMD module of Discover Studio 3.5. CHARMm force field and temperature of 300 K were adopted, and the simulation time was set as 20 ns. Binding energies were calculated employing the internal scoring module of Discovery Studio 3.5.[28,29]

Determination of Optimum pH and Stability of ^{WT}*Kp*ADH and *Kp*ADH$_{V84I/Y127M}$. Effects of pH on the activities of purified ^{WT}*Kp*ADH and *Kp*ADH$_{V84I/Y127M}$ were determined employing the above-mentioned standard activity assay except for different buffers with pH ranging from 6.0 to 8.0 (PBS buffer) and 8.0 to 10.0 (glycine-NaOH buffer). Purified ^{WT}*Kp*ADH and *Kp*ADH$_{V84I/Y127M}$ (1.0 mg·mL^{-1}) were incubated in buffers of pH 9.0 and 9.5 at 30 °C. Aliquot samples (10 μL) were withdrawn at intervals, and activities were determined employing the standard activity assay method. All activities were determined in triplicate.

RESULTS AND DISCUSSION

Identifying Key Residues of *Kp*ADH by MD Simulations. The kinetic parameters of purified *Kp*ADH toward 1,4-BD and 2-HTHF were determined in order to better understand its enzymatic characteristics. The K_M, k_{cat}, and k_{cat}/K_M of *Kp*ADH toward 1,4-BD were 50.6 mM, 8.76 min^{-1}, and 0.173 $min^{-1}\cdot mM^{-1}$ (Table 2), respectively, while the K_M, k_{cat}, and k_{cat}/K_M toward 2-HTHF were 2.23 mM, 2.63 × 10^3 min^{-1}, and 1.18 × 10^3 $min^{-1}\cdot mM^{-1}$ (Table 4), respectively. The oxidation of 1,4-BD was the rate-limiting step, and the low k_{cat}/K_M of this step was undesirable for the efficient regeneration of NADPH. Remarkably, the k_{cat}/K_M toward 2-HTHF was 6.82 × 10^3-fold higher than that of 1,4-BD, and the unmatched k_{cat}/K_M values between step 1 and step 2 were also unfavorable for the NADPH regeneration. Consequently, *Kp*ADH was engineered to increase its k_{cat}/K_M value toward 1,4-BD and to balance the kinetics between 1,4-BD and 2-HTHF.

DOI: 10.1021/acssuschemeng.9b03879
ACS Sustainable Chem. Eng. 2019, 7, 15706−15714

*Kp*ADH displays low sequence similarity to the enzymes deposited in NCBI, with the highest identity of only 54.5%. Moreover, homologous enzymes, such as Gre2p and CgKR1, could not catalyze the oxidation of isopropanol or 1,4-BD.[30,31] Fortunately, the crystal structure of wild type *Kp*ADH docked with 1,4-BD was available (^{WT}*Kp*ADH, PDB: 5Z2X), and this structure was used in a molecular dynamic (MD) simulation of 20 ns to identify key residues that may affect the binding and catalytic activity of *Kp*ADH toward 1,4-BD. The average conformation was extracted as shown in Figure 1. Distance

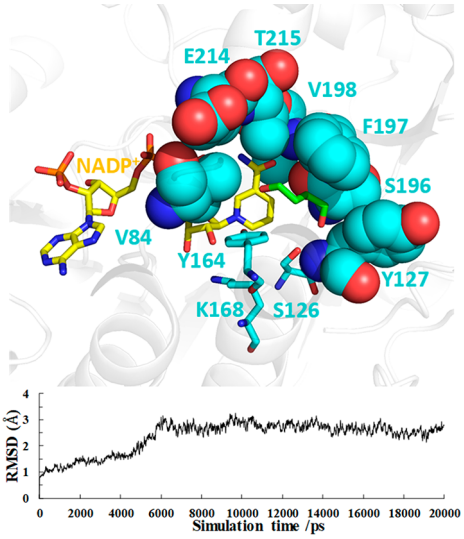

Figure 1. Analysis of the substrate binding pockets of ^{WT}*Kp*ADH using MD simulations. Yellow sticks: NADP$^+$, blue sticks: catalytic triad, green sticks: 1,4-BD, blue spheres: V84, Y127, S196, F197, V198, E214, and T215.

analysis demonstrated that 1,4-BD was surrounded by residues V84, Y127, S196, F197, V198, E214, and T215. The distances between 1,4-BD and residues V84, Y127, and S196 were less than 3.0 Å. Notably, residue Y127, which is 2.2 Å from 1,4-BD, might produce significant steric hindrance. Consensus analysis of the above-mentioned residues was carried out for ADHs of various origins (Figure S1). With the exception of a strictly conserved residue T215, the other six residues were analyzed for their roles in binding and oxidizing of 1,4-BD.

Engineering *Kp*ADH for Improved Activity toward 1,4-BD. Each residue was subjected to saturation mutagenesis and high throughput screening with 1,4-BD as the substrate and NADP$^+$ as a cofactor (Figure S2). All variants of V198 and E214 displayed decreased activity toward 1,4-BD compared with ^{WT}*Kp*ADH. The variants that showed the highest potential activity in each library were *Kp*ADH$_{V84I}$, *Kp*ADH$_{Y127C}$, *Kp*ADH$_{Y127M}$, *Kp*ADH$_{S196A}$, and *Kp*ADH$_{F197W}$, with relative activities of 392%, 261%, 248%, 118%, and 120%, respectively (Figure 2). The relative activities of purified *Kp*ADH$_{V84I}$, *Kp*ADH$_{Y127C}$, *Kp*ADH$_{Y127M}$, *Kp*ADH$_{S196A}$, and *Kp*ADH$_{F197W}$ toward isopropanol were 21.7%, 22.8%, 105%, 93.0%, and 19.6%, respectively. Only *Kp*ADH$_{Y127M}$ exhibited increased activities toward both 1,4-BD and isopropanol. Variant *Kp*ADH$_{V84I}$ exhibited the highest activity for the oxidation of 1,4-BD among all single mutants.

In order to gain insight into the binding affinity and catalytic efficiency of the variants, their kinetic parameters were determined according to the ordered Bi−Bi kinetic model.[32]

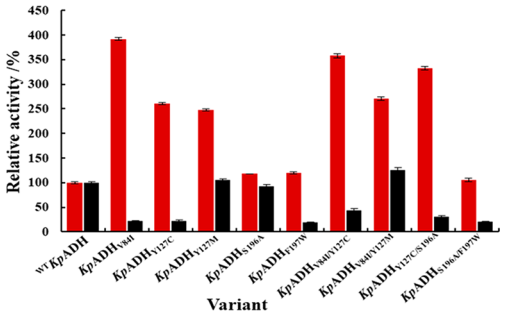

Figure 2. Relative activities of ^{WT}*Kp*ADH and variants toward 1,4-BD and isopropanol. Red bar: 1,4-BD, black bar: isopropanol.

As shown in Table 2, *Kp*ADH$_{V84I}$ displayed a k_{cat} of 80.3 min^{-1}, which was 9.17-fold higher than ^{WT}*Kp*ADH, suggesting residue 84 is vital for the oxidation activity toward 1,4-BD. However, a higher K_M toward 1,4-BD and NADP$^+$ was observed in *Kp*ADH$_{V84I}$, 1.71- and 1.96-fold higher than that of ^{WT}*Kp*ADH, respectively, which is suggestive of a weaker substrate binding affinity toward 1,4-BD and NADP$^+$. As a result, the k_{cat}/K_M of *Kp*ADH$_{V84I}$ toward 1,4-BD was 5.36-fold higher than ^{WT}*Kp*ADH.

The k_{cat} values of *Kp*ADH$_{Y127C}$ and *Kp*ADH$_{Y127M}$ were 2.07- and 3.70-fold higher than that of ^{WT}*Kp*ADH, and their apparent K_M values toward 1,4-BD were 21.4 mM and 28.9 mM, respectively, both of which were lower than that of ^{WT}*Kp*ADH (50.6 mM); *Kp*ADH$_{Y127C}$ and *Kp*ADH$_{Y127M}$ also displayed a decrease K_M toward NADP$^+$ (52.8% and 93.0%) in contrast with that of ^{WT}*Kp*ADH. The kinetics data demonstrated that residue Y127 was critical in both catalytic efficiency and binding of 1,4-BD and NADP$^+$. The k_{cat}/K_M of *Kp*ADH$_{Y127M}$ toward 1,4-BD was 1.12 min^{-1}·M^{-1}, a 6.47-fold increase over that of ^{WT}*Kp*ADH. The k_{cat}/K_M values of *Kp*ADH$_{S196A}$ and *Kp*ADH$_{F197W}$ were improved to 0.301 min^{-1}·mM^{-1} and 0.673 min^{-1}·mM^{-1}, respectively. On the basis of the above results, residue V84 appears to play an important role in catalytic efficiency, while Y127 seems crucial for both catalytic efficiency and binding of 1,4-BD and NADP$^+$ in the rate-limiting step.

Combinatorial mutagenesis was then performed to further improve the activity of the selected variants *Kp*ADH$_{V84I/Y127C}$, *Kp*ADH$_{V84I/Y127M}$, *Kp*ADH$_{Y127C/S196A}$, and *Kp*ADH$_{S196A/F197W}$ (Figure 2). The relative activities of *Kp*ADH$_{V84I/Y127C}$ and *Kp*ADH$_{V84I/Y127M}$ toward 1,4-BD were 358% and 271%, while toward isopropanol they were 43.7% and 126%, respectively. Variant *Kp*ADH$_{V84I/Y127C}$ exhibited the highest activity among all double mutants but still had lower activity than that of *Kp*ADH$_{V84I}$. It is worth mentioning that *Kp*ADH$_{V84I/Y127M}$ displayed improved activity toward both 1,4-BD and isopropanol, similar to *Kp*ADH$_{Y127M}$. Considering the limited effect of the F197W mutation on oxidative activity and the negative effect of the S196A mutation on thermal stability (data not shown), triple combinatorial mutagenesis was not explored.

Because of its decreased K_M (31.0 mM) and increased k_{cat} (28.7 min^{-1}) toward 1,4-BD, the k_{cat}/K_M of the double mutant *Kp*ADH$_{Y127C/S196A}$ was 0.926 min^{-1}·mM^{-1} (Table 2), which was 1.09- and 3.08-fold above those of *Kp*ADH$_{Y127C}$ and *Kp*ADH$_{S196A}$, respectively, indicating a synergistic effect of the Y127C and S196A mutations. With regard to variant *Kp*ADH$_{S196A/F197W}$, a decreased K_M (23.4 mM) and a slightly

DOI: 10.1021/acssuschemeng.9b03879
ACS Sustainable Chem. Eng. 2019, 7, 15706−15714

Table 3. Kinetic Parameters of ^{WT}*Kp*ADH and Variants toward Different Diols

Variant	HO⁓OH			HO⁓⁓OH		
	K_M [mM]	k_{cat} [min^{-1}]	k_{cat}/K_M [min^{-1}·mM^{-1}]	K_M [mM]	k_{cat} [min^{-1}]	k_{cat}/K_M [min^{-1}·mM^{-1}][a]
^{WT}*Kp*ADH	74.4±2.2	55.7±1.0	0.75±0.01	18.5±1.5	41.9±0.9	2.27±0.10
*Kp*ADH$_{V84I}$	42.5±1.5	51.1±0.8	1.20±0.02**	12.3±0.7	64.7±1.7	5.25±0.16**
*Kp*ADH$_{Y127C}$	63.5±0.1	25.1±0.9	0.39±0.01**	31.8±1.7	36.2±2.2	1.14±0.01**
*Kp*ADH$_{Y127M}$	14.3±0.9	46.6±1.7	3.27±0.09**	6.50±0.5	39.5±1.9	6.09±0.17**
*Kp*ADH$_{S196A}$	75.4±2.3	64.4±1.6	0.86±0.01*	21.3±2.6	46.4±0.8	2.18±0.13*
*Kp*ADH$_{F197W}$	61.2±1.9	40.1±1.2	0.66±0.01*	13.5±0.1	26.2±1.2	1.94±0.07**
*Kp*ADH$_{V84I/Y127C}$	16.3±0.8	24.8±1.1	1.52±0.01**	12.9±1.3	98.3±2.5	7.63±0.15**
*Kp*ADH$_{V84I/Y127M}$	8.20±0.2	19.3±0.9	2.35±0.05**	6.50±1.0	75.2±2.1	11.5±0.15**
*Kp*ADH$_{Y127C/S196A}$	43.2±0.5	23.7±0.7	0.55±0.01**	21.6±1.0	49.8±1.4	2.31±0.04*
*Kp*ADH$_{S196A/F197W}$	50.1±0.5	43.1±1.3	0.86±0.02*	10.7±0.8	35.7±0.7	3.34±0.18**

[a]Statistical analysis was performed: * indicates a statistically significant difference ($p < 0.05$), ** indicates an extremely significant difference ($p < 0.01$).

enhanced k_{cat} (10.2 min^{-1}) were found, giving a k_{cat}/K_M toward 1,4-BD of 0.436 min^{-1}·mM^{-1}, and the combination of two adjacent residues (S196A and F197W) did not play a cooperative role. Compared with *Kp*ADH$_{V84I}$ and *Kp*ADH$_{Y127C}$, double mutant *Kp*ADH$_{V84I/Y127C}$ displayed a further increased k_{cat}/K_M of 1.30 min^{-1}·mM^{-1}, which was 7.51-fold above that of ^{WT}*Kp*ADH. As shown in Table 2, the highest k_{cat}/K_M value toward 1,4-BD of 2.00 min^{-1}·mM^{-1} was observed with *Kp*ADH$_{V84I/Y127M}$, 11.6-fold higher than that of ^{WT}*Kp*ADH. Both a significant decrease in K_M value (50.6 mM to 15.1 mM) and an increase in k_{cat} value (8.76 min^{-1} to 30.1 min^{-1}) contributed to the remarkably improved k_{cat}/K_M of *Kp*ADH$_{V84I/Y127M}$ toward 1,4-BD. Owing to the positive effect of Y127M mutation on substrate binding, the K_M of *Kp*ADH$_{V84I/Y127M}$ toward 1,4-BD was over 5 times lower than that of *Kp*ADH$_{V84I}$. In addition, *Kp*ADH$_{V84I/Y127M}$ also showed the best affinity toward NADP$^+$, the K_M toward NADP$^+$ decreased from 15.8 mM (^{WT}*Kp*ADH) to 3.05 mM. Consequently, Y127 was shown to be a key residue that could coordinate with other residues in enhancing the binding affinity of substrate. Importantly, no substrate inhibition was detected in all tested single and double mutants, even at 250 mM 1,4-BD. The K_{ia} values, dissociation constants toward NADP$^+$, of most mutants improved to varying degrees, indicating increased binding to noncatalytic site, but there was no significant effect on affinity of NADP$^+$ observed from the apparent K_M toward NADP$^+$, in the rate-limiting step for oxidation of 1,4-BD.

Analysis of the Substrate Specificities of ^{WT}*Kp*ADH and Variants. Kinetic parameters of ^{WT}*Kp*ADH and other variants toward 1,5-pentanediol (1,5-PD) and 1,6-hexanediol (1,6-HD) were also investigated (Table 3). The k_{cat}/K_M values of ^{WT}*Kp*ADH toward 1,5-PD and 1,6-HD were 0.75 min^{-1}·mM^{-1} and 2.27 min^{-1}·mM^{-1}, respectively, representing 4.34- and 13.1-fold increases compared 1,4-BD. The result suggests that diols with a longer chain length than 1,4-BD could be more efficiently oxidized by *Kp*ADH. Compared with 1,4-BD, the K_M values of *Kp*ADH$_{V84I}$ toward 1,5-PD and 1,6-HD were reduced by 50.9% (42.5 mM) and 85.8% (12.3 mM), respectively, indicating the positive role of *Kp*ADH$_{V84I}$ in enhancing the binding affinity of longer chain diols. However, *Kp*ADH$_{Y127C}$ had a greatly decreased k_{cat}/K_M and was found to be unfavorable for the oxidation of 1,5-PD and 1,6-HD. Unlike *Kp*ADH$_{Y127C}$, the *Kp*ADH$_{Y127M}$ displayed a remarkable effect on binding affinity. The K_M values of *Kp*ADH$_{Y127M}$ toward 1,5-PD and 1,6-HD were decreased to 14.3 mM and 6.50 mM, respectively, which represented a reduction of 80.8% and 64.9% compared to those of ^{WT}*Kp*ADH. As a result, the k_{cat}/K_M of *Kp*ADH$_{Y127M}$ toward 1,5-PD and 1,6-HD reached 3.27 min^{-1}·mM^{-1} and 6.09 min^{-1}·mM^{-1}, respectively, which were 4.36- and 2.68-fold higher than ^{WT}*Kp*ADH.

Mutations of S196 into Ala and F197 into Trp had little influence on the oxidization of 1,5-PD and 1,6-HD. With regard to double mutant *Kp*ADH$_{V84I/Y127M}$, the K_M values toward 1,5-PD and 1,6-HD were further decreased to 8.20 mM and 6.50 mM, respectively, which were merely 11.0% and 35.1% of those of ^{WT}*Kp*ADH. The corresponding k_{cat}/K_M values were 2.35 min^{-1}·mM^{-1} and 11.5 min^{-1}·mM^{-1}. These values represented 3.13- and 5.07-fold increases over ^{WT}*Kp*ADH. Interestingly, the k_{cat}/K_M of *Kp*ADH$_{V84I/Y127M}$ toward tested diols obeyed the observed sequence of 1,6-HD > 1,5-PD > 1,4-BD, which was consistent with ^{WT}*Kp*ADH. Only CDX-019, *Lb*ADH, and *Te*SADH have been reported to be able to catalyze the oxidation of 1,6-HD for NAPDH regeneration, with V_{max} of 0.1, 0.4, and 0.4 μmol·min^{-1}·mg^{-1}, respectively.[21] The V_{max} values of *Kp*ADH$_{V84I/Y127C}$ and *Kp*ADH$_{V84I/Y127M}$ were calculated to be 2.34 and 1.79 μmol·min^{-1}·mg^{-1}, which were almost 5 times higher than the highest reported. On the basis of its remarkable kinetic parameters, variant *Kp*ADH$_{V84I/Y127M}$ could be a promising NADPH regeneration system utilizing diols as "smart cosubstrates".

Comparison of Different Cofactor Regeneration Systems. Cofactor regeneration systems with diols as "smart cosubstrates" have been successfully demonstrated in the coupled reactions catalyzed by NADH-dependent enoate reductase from *Thermus scotoductus* SA-01 (*Ts*ER), 3-hydroxybenzoate-6-hydroxylase from *Rhodococcus jostii* RHA1 (3HB6H), and Baeyer−Villiger monooxygenase from *Acinetobacter* sp. NCIMB 9871 (BVMO).[19,22] Herein, the application potential of this newly developed NADPH regeneration system was evaluated by coupling it to a NADPH-dependent amino acid dehydrogenase from *Ureibacillus thermosphaericus*

DOI: 10.1021/acssuschemeng.9b03879
ACS Sustainable Chem. Eng. 2019, 7, 15706−15714

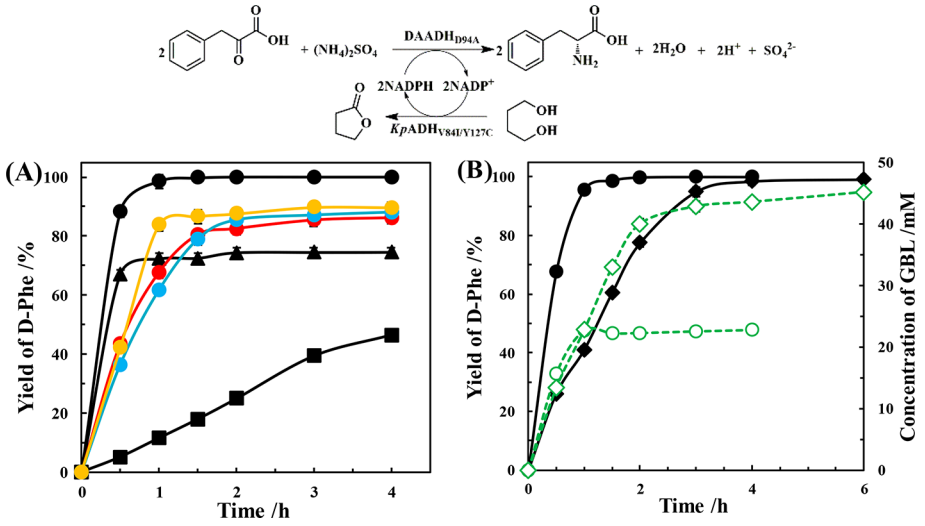

Figure 3. Asymmetric preparation of D-Phe with DAADH$_{D94A}$ coupled with NADPH regeneration approaches. (A) Effect of different cofactor regeneration systems. (●) *Kp*ADH$_{V84I/Y127M}$, (solid red circle) *Kp*ADH$_{V84I}$, (solid blue circle) *Kp*ADH$_{Y127C}$, (solid yellow circle) *Kp*ADH$_{V84I/Y127C}$, (■) ^{WT}*Kp*ADH, (▲) GDH. Reactions were performed with 0.5 mM NADP$^+$, 50 mM PPA, 50 mM 1,4-BD, or 100 mM glucose, 1.5 kU·L^{-1} enzymes, and 5 kU·L^{-1} DAADH$_{D94A}$. (B) Production of D-Phe and GBL at different PPA and 1,4-BD concentrations employing *Kp*ADH$_{V84I/Y127M}$. (●) and (○) concentrations of D-Phe and GBL at 50 mM PPA and 25 mM 1,4-BD, (◆) and (◇) concentrations of D-Phe and GBL at 100 mM PPA and 50 mM 1,4-BD.

Table 4. Kinetic Parameters of ^{WT}*Kp*ADH and Variants toward NADP$^+$ and 2-HTHF

variant	K_{ia} [μM][a]	$K_{M,\ NADP+}$ [μM]	$K_{M,\ 2\text{-HTHF}}$ [mM]	k_{cat} [$\times 10^3$ min^{-1}]	k_{cat}/K_M to HTHF [min^{-1}·mM^{-1}][b]	fold change[c]
^{WT}*Kp*ADH	57.9 ± 6.2	64.8 ± 2.6	2.23 ± 0.37	2.63 ± 0.09	1.18 ± 0.15 × 10^3	6.82 × 10^3
*Kp*ADH$_{V84I}$	108 ± 23	159 ± 18	1.90 ± 0.96	1.33 ± 0.20	700 ± 148*	755
*Kp*ADH$_{Y127C}$	361 ± 27	107 ± 9	2.40 ± 0.71	0.464 ± 0.04	193 ± 40**	228
*Kp*ADH$_{Y127M}$	129 ± 14	76.8 ± 15.6	5.90 ± 2.19	2.34 ± 0.39	397 ± 81**	354
*Kp*ADH$_{S196A}$	217 ± 34	456 ± 31	1.55 ± 0.65	2.27 ± 0.27	1.46 ± 0.11 × 10^3*	4.86 × 10^3
*Kp*ADH$_{F197W}$	163 ± 11	107 ± 5	1.59 ± 0.30	1.09 ± 0.05	686 ± 77**	1.02 × 10^3
*Kp*ADH$_{V84I/Y12C}$	961 ± 99	462 ± 57	4.70 ± 2.88	0.315 ± 0.07	67.0 ± 16.0**	51.6
*Kp*ADH$_{V84I/Y127M}$	94.0 ± 7.2	80.7 ± 7.7	4.39 ± 0.92	0.855 ± 0.06	195 ± 27**	97.8
*Kp*ADH$_{Y127C/S196A}$	288 ± 26	565 ± 59	6.38 ± 2.50	0.374 ± 0.07	58.6 ± 12**	63.3
*Kp*ADH$_{S196A/F197W}$	111 ± 7	100 ± 3	0.85 ± 0.11	0.441 ± 0.01	519 ± 55**	1.19 × 10^3

[a] K_{ia} denotes the dissociation constant toward NADP$^+$. [b] Statistic analysis was performed: * indicates a statistically significant difference ($p < 0.05$), ** indicates an extremely significant difference ($p < 0.01$). [c] Fold change denotes the ratio of k_{cat}/K_M toward 2-HTHF to k_{cat}/K_M toward 1,4-BD.

(DAADH$_{D94A}$).[33] DAADH$_{D94A}$ catalyzed the asymmetric reduction of phenylpyruvic acid (PPA) into D-phenylalanine (D-Phe), an important chiral building block for nateglinide (a drug for type II diabetes).[34]

Cofactor regeneration with 1,4-BD and glucose as cosubstrates were initially tested at 50 mM PPA. 1,4-BD and glucose were added in 1.0 equiv and 2.0 equiv relative to the substrate. ^{WT}*Kp*ADH, *Kp*ADH$_{V84I/Y127M}$, and glucose dehydrogenase (GDH) were added to the level of equivalent activities (1.5 kU·L^{-1}). As illustrated in Figure 3A, the yield of D-Phe reached 72.1 ± 1.9% after 1 h and slightly increased to 74.4 ± 1.6% after 4 h employing GDH for cofactor regeneration. Without pH adjustment, the pH of the reaction declined to lower than 6.0 because of the gluconic acid produced, which was disadvantageous for the reaction since the optimal pH of DAADH$_{D94A}$ in the asymmetric reduction was pH 9.0. The conversion curve employing *Kp*ADH$_{V84I/Y127M}$ was distinct from that of ^{WT}*Kp*ADH. With ^{WT}*Kp*ADH, the yield of D-Phe was 46.4 ± 1.9% at 4 h, and a slightly higher conversion of 50% was obtained after further reaction time. For *Kp*ADH$_{V84I/Y127M}$, the initial reaction rate was so high that the conversion reached 98.5 ± 2.3% in 1 h. PPA was completely converted into D-Phe in 4 h. As previously mentioned, the conversion of 1,4-BD into GBL is irreversible and thermodynamically favored. Moreover, the optimum pH for both ^{WT}*Kp*ADH and *Kp*ADH$_{V84I/Y127M}$ was determined to be pH 9.5 (Figure S19), which was much more favorable for DAADH$_{D94A}$ than GDH. Also, *Kp*ADH$_{V84I/Y127M}$ exhibited greater stability than ^{WT}*Kp*ADH at pH 9.5 (Figure S20).

The k_{cat}/K_M of *Kp*ADH$_{V84I/Y127M}$ toward 2-HTHF in step 2 was 195 min^{-1}·mM^{-1} (Table 4). It is worth noting that the ratio of k_{cat}/K_M toward 2-HTHF and 1,4-BD was 97.8, which is nearly 70-fold lower than that of ^{WT}*Kp*ADH (k_{cat}/K_M of 6.82 × 10^3). To investigate the significance of the ratio of k_{cat}/K_M between 2-HTHF and 1,4-BD, variants *Kp*ADH$_{V84I/Y127C}$, *Kp*ADH$_{Y127C}$, and *Kp*ADH$_{V84I}$ (k_{cat}/K_M ratios of 51.6, 228, and 775) were also applied as NADPH regeneration systems at the same enzyme loading of 1.5 kU·L^{-1}. A higher yield of 83.7% was observed with *Kp*ADH$_{V84I/Y127C}$ at 1 h, which might be due to its higher k_{cat}/K_m toward 1,4-BD. Similar yields were obtained at 1 h (61.6% and 67.6%) with *Kp*ADH$_{Y127C}$ and *Kp*ADH$_{V84I}$, which exhibited similar k_{cat}/K_M toward 1,4-BD. Among variants with k_{cat}/K_M ratios of 51.6−6.82 × 10^3 tested, *Kp*ADH$_{V84I/Y127M}$ possessed a k_{cat}/K_M ratio of around 100 and

DOI: 10.1021/acssuschemeng.9b03879
ACS Sustainable Chem. Eng. 2019, 7, 15706−15714

was shown to be an appropriate reaction system for the sequential oxidation of 1,4-BD into GBL. Consequently, both improved catalytic efficiency and balanced k_{cat}/K_M between 1,4-BD and 2-HTHF contributed to the high efficiency in reductive amination of PPA into D-Phe.

Application of *Kp*ADH$_{V84I/Y127M}$ in the Synthesis of D-Phe. Since the sequential oxidation of one 1,4-BD molecule produced 2 equiv of NADPH, the addition of 1,4-BD was further reduced to 0.5 equiv of the substrate in the *Kp*ADH$_{V84I/Y127M}$ NADPH regeneration system. As shown in Figure 3B, the initial production of D-Phe was 67.6 ± 1.5% at 0.5 h, 20.7% lower than that with 1,4-BD at 1.0 equiv of PPA (50 mM) (Figure 3A), which indicated that a higher amount of cosubstrate was advantageous for NADPH regeneration. With 25 mM 1,4-BD, the yield of D-Phe reached 99.8 ± 1.0% in 2 h at 50 mM PPA. The production of the coproduct GBL, an important solvent, was determined to be 22.8 mM at 4 h. As a result, in comparison to the substrate, 0.5 equiv of 1,4-BD was adequate for the bioreduction system. When PPA loading was further increased to 100 mM, the addition of 1,4-BD was also increased to 50 mM. The yield of D-Phe increased rapidly to 95.0 ± 1.7% in the first 3 h. The production of D-Phe then slowly increased to 99.2 ± 1.5% after 6 h, along with 45.2 mM GBL produced. Enantioselectivity analysis revealed that the *e.e.* value of D-Phe produced was over 99.9%. The turnover frequency (TOF) value of *Kp*ADH$_{V84I/Y127M}$ was calculated to be 3.7 min^{-1}, which was a TOF value 2.0-fold higher than *Te*SADH using 1,6-hexanediol as a cosubstrate at the same concentration.[22] Considering the basic pH preference of DAADH$_{D94A}$, the traditional strategy was found to be at the expense of a high loading of GDH. The highest observed conversion for preparing D-Phe was achieved with a variant of *meso*-DAPDH from *Symbiobacterium thermophilum*. As much as 100 mM PPA was converted with an efficiency of 96.9% conversion after 24 h with the assistance of 0.2 g·L^{-1} GDH (*c.a.* 36 KU·L^{-1}).[35,36] This newly developed cofactor regeneration system employing *Kp*ADH$_{V84I/Y127M}$ was more advantageous in NADPH regeneration for amino acid dehydrogenase. Optimizing on the regeneration of NADPH with 1,6-HD is also undergoing, since *Kp*ADH$_{V84I/Y127M}$ displays a much higher efficiency than 1,4-BD.

Elucidating the Mechanism of Enhanced Activity toward 1,4-BD. Virtual mutation and MD simulation were conducted to explore the molecular basis of the improved activity and balanced k_{cat}/K_M. After MD simulation of 20 ns, the average conformations were extracted. The interactions and binding energies were also calculated. In the conformation of ^{WT}*Kp*ADH in complex with 1,4-BD, only one hydrogen bond between Tyr164 and 1,4-BD was identified (Figure 4A). It is presumed that the bulky Tyr127 residue might block the binding and rotation of 1,4-BD. Moreover, no interaction was found between Ser126 and 1,4-BD, and Ser126 had been shown to be essential for stabilizing the substrate.[37,38] However, more hydrogen bonds were predicted in the *Kp*ADH$_{V84I/Y127M}$ complex, although no directed interaction was found between 1,4-BD and *Kp*ADH$_{V84I/Y127M}$. The substrate binding pocket of *Kp*ADH$_{V84I/Y127M}$ had a tendency to become a little larger and more hydrophobic than that of ^{WT}*Kp*ADH. The enhanced hydrophobicity of Ile84 was shown to have pushed 1,4-BD toward the bottom of the substrate binding pocket, while the mutation of Y127M increased the binding pocket volume. These changes gave rise to the two possible extra hydrogen bonds between Ser126 (or Ala128) and the hydroxyl group of 1,4-BD (Figure 4B, detailed interactions can be found in Figure S13 and Figure S14). The binding energy between *Kp*ADH$_{V84I/Y127M}$ and 1,4-BD was calculated to be −81.6 kcal·mol^{-1}, much lower than −70.0 kcal·mol^{-1} of ^{WT}*Kp*ADH. Interactions between *Kp*ADH and 2-HTHF could be found in Figure 4C, including hydrogen bonds with Ser126 or Tyr164, π-alkyl interaction with Phe197, and alky−alkyl interaction with Ala128. The intricate binding network between *Kp*ADH and 2-HTHF led to a high k_{cat}/K_M toward 2-HTHF. The binding energy was calculated to be −102.7 kcal·mol^{-1}. The altered hydrophobicity of the substrate binding pocket also resulted in the movement of 2-HTHF toward the bottom. Because of the longer length of 2-HTHF than 1,4-BD, the movement led to an extended distance (4.1 Å) between Ser126 and 2-HTHF, which was unfavorable for the formation of hydrogen bonds. However, other interactions between Tyr164, Ala128, and Phe197 were still present (Figure 4D). As a result, the binding energy between variant *Kp*ADH$_{V84I/Y127M}$ and 2-HTHF was reduced to −89.3 kcal·mol^{-1}, and the k_{cat}/K_M was decreased, as shown in Table 4. As mentioned above, the mutation of Val84 and Tyr127 into Ile and Met altered the spatial structure and hydrophobicity of the substrate binding pocket. The substrates might better access the bottom of the substrate binding pocket with changes in the hydrogen-bonding network, varying from 1,4-BD and 2-HTHF.

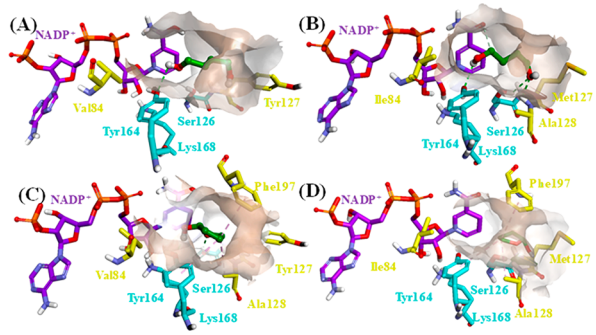

Figure 4. Analysis of the substrate binding mode in ^{WT}*Kp*ADH and *Kp*ADH$_{V84I/Y127M}$ using MD simulations. (A) ^{WT}*Kp*ADH in complex with 1,4-BD, (B) *Kp*ADH$_{V84I/Y127M}$ with 1,4-BD, (C) ^{WT}*Kp*ADH with 2-HTHF, and (D) *Kp*ADH$_{V84I/Y127M}$ with 2-HTHF. NADP$^+$ was depicted with purple sticks, catalytic triad (Ser126-Tyr164-Lys168) with blue sticks, residues 84 and 127 and other residues participating in the substrate binding with yellow sticks, 1,4-BD and 2-HTHF with green balls and sticks.

CONCLUSIONS

The alcohol dehydrogenase *Kp*ADH was engineered for improved NADPH regeneration employing 1,4-BD as a "smart cosubstrate". Key residues were identified by molecular dynamics and subjected to saturational and combinatorial mutagenesis. Residues V84 and Y127 were shown to play essential roles in the catalytic efficiency and substrate binding affinity, and mutations to these key residues favorably altered the substrate binding pocket and enhanced the hydrogen-bonding network between the mutant enzyme and 1,4-BD. In the rate-limiting step, the k_{cat}/K_M of *Kp*ADH$_{V84I/Y127M}$ toward 1,4-BD was 2.00 min^{-1}·mM^{-1}, 11.6-fold higher than ^{WT}*Kp*ADH. Moreover, the ratio of k_{cat}/K_M toward 2-HTHF versus 1,4-BD was dramatically reduced to 97.8 from 6.82 × 10^3 in ^{WT}*Kp*ADH, which was favorable for the sequential

DOI: 10.1021/acssuschemeng.9b03879
ACS Sustainable Chem. Eng. 2019, 7, 15706−15714

oxidation of 1,4-BD. Variant *Kp*ADH$_{V84I/Y127M}$ was applied in a coupled reaction for NADPH regeneration. As much as 100 mM PPA was converted into D-Phe with a 99.2% yield employing 50 mM 1,4-BD. This enhancement was ascribed to the improved catalytic efficiency toward 1,4-BD and the balanced k_{cat}/K_M between 1,4-BD and 2-HTHF. This study has demonstrated the engineering and utilization capacity of ADH as an efficient NADPH regeneration system employing diols as "smart cosubstrates".

■ ASSOCIATED CONTENT

Supporting Information

The Supporting Information is available free of charge on the ACS Publications website at DOI: 10.1021/acssuschemeng.9b03879.

Table S1, primers used in this study; Figure S1, consensus analysis; Figure S2, HTS results; Figures S3−S12, purification of variants; Figures S13−S14, substrate binding pocket analysis; Figures S15−S16, calibration curves; Figures S17−S18, kinetic parameters analysis by Matlab software; Figures S19−S21, optimal pH and thermal stability of ^{WT}*Kp*ADH and *Kp*ADH$_{V84I/Y127M}$ (PDF)

■ AUTHOR INFORMATION

Corresponding Author

*E-mail: yni@jiangnan.edu.cn.

ORCID

Ye Ni: 0000-0003-4887-7517

Author Contributions

#(G.C.X., C.Z.) These authors contributed equally to this work.

Notes

The authors declare no competing financial interest.

■ ACKNOWLEDGMENTS

We are grateful to the National Key Research and Development Program (2018YFA0901700), the National Natural Science Foundation of China (21506073, 21776112), the National First-Class Discipline Program of Light Industry Technology and Engineering (LITE2018-07), the Natural Science Foundation of Jiangsu Province (BK20171135), the Program of Introducing Talents of Discipline to Universities (111-2-06), and Top-notch Academic Programs Project of Jiangsu Higher Education Institutions for the financial support of this research.

■ ABBREVIATIONS

1,4-BD, 1,4-butanediol; 2-HTHF, 2-hydroxytetrahydrofuran; GBL, γ-butyrolactone; 1,5-PD, 1,5-pentanediol; 1,6-HD, 1,6-hexanediol; TOF, turnover frequency; PPA, phenylpyruvic acid; D-Phe, D-phenylalanine

■ REFERENCES

(1) Bornscheuer, U. T.; Huisman, G. W.; Kazlauskas, R. J.; Lutz, S.; Moore, J. C.; Robins, K. Engineering the Third Wave of Bocatalysis. *Nature* **2012**, *485*, 185−194.

(2) Sheldon, R. A.; Woodley, J. M. Role of Biocatalysis in Sustainable Chemistry. *Chem. Rev.* **2018**, *118*, 801−838.

(3) Savile, C. K.; Janey, J. M.; Mundorff, E. C.; Moore, J. C.; Tam, S.; Jarvis, W. R.; Colbeck, J. C.; Krebber, A.; Fleitz, F. j.; Brands, J.; Devine, P. N.; Huisman, G. W.; Hughes, G. J. Biocatalytic Asymmetric Synthesis of Chiral Amines from Ketones Applied to Sitagliptin Manufacture. *Science* **2010**, *329*, 305−309.

(4) Hollmann, F.; Arends, I. W. C. E.; Holtmann, D. Enzymatic Reductions for the Chemist. *Green Chem.* **2011**, *13*, 2285−2314.

(5) Cheng, J.; Xu, G. C.; Han, R. Z.; Dong, J. J.; Ni, Y. Efficient Access to L-Phenylglycine Using a Newly Identified Amino Acid Dehydrogenase from *Bacillus clausii*. *RSC Adv.* **2016**, *6*, 80557−80563.

(6) Hollmann, F.; Arends, I. W. C. E.; Buehler, K.; Schallmey, A.; Buehler, B. Enzyme-Mediated Oxidations for the Chemist. *Green Chem.* **2011**, *13*, 226−265.

(7) Magano, J.; Dunetz, J. R. , Large-scale Carbonyl Reductions in the Pharmaceutical Industry. *Org. Process Res. Dev.* **2012**, *16*, 1156−1184.

(8) Huisman, G. W.; Liang, J.; Krebber, A. Practical Chiral Alcohol Manufacture Using Ketoreductases. *Curr. Opin. Chem. Biol.* **2010**, *14*, 122−129.

(9) Zhao, H. M.; van der Donk, W. A. Regeneration of Cofactors for Use in Biocatalysis. *Curr. Opin. Biotechnol.* **2003**, *14*, 583−589.

(10) Kara, S.; Schrittwieser, J. H.; Hollmann, F.; Ansorge-Schumacher, M. B. Recent Trends and Novel Concepts in Cofactor-Dependent Biotransformations. *Appl. Microbiol. Biotechnol.* **2014**, *98*, 1517−1529.

(11) Moore, J. C.; Pollard, D. J.; Kosjek, B.; Devine, P. N. Advances in the Enzymatic Reduction of Ketones. *Acc. Chem. Res.* **2007**, *40*, 1412−1419.

(12) Liu, W.; Wang, P. Cofactor Regeneration for Sustainable Enzymatic Biosynthesis. *Biotechnol. Adv.* **2007**, *25*, 369−384.

(13) Ni, Y.; Holtmann, D.; Hollmann, F. How Green is Biocatalysis? To Calculate is to Know. *ChemCatChem* **2014**, *6*, 930−943.

(14) Hummel, W.; Groger, H. Strategies for regeneration of nicotinamide coenzymes emphasizing self-sufficient closed-loop recycling systems. *J. Biotechnol.* **2014**, *191*, 22−31.

(15) Aksu, S.; Arends, I. W. C. E.; Hollmann, F. A New Regeneration System for Oxidized Nicotinamide Cofactors. *Adv. Synth. Catal.* **2009**, *351*, 1211−1216.

(16) Broussy, S.; Cheloha, R. W.; Berkowitz, D. B. Enantioselective, Ketoreductase-Based Entry into Pharmaceutical Building Blocks: Ethanol as Tunable Nicotinamide Reductant. *Org. Lett.* **2009**, *11*, 305−308.

(17) Schroer, K.; Tacha, E.; Luetz, S. Process Intensification for Substrate-Coupled Whole cell Ketone Reduction by *in situ* Acetone Removal. *Org. Process Res. Dev.* **2007**, *11*, 836−841.

(18) Kara, S.; Spickermann, D.; Schrittwieser, J. H.; Weckbecker, A.; Leggewie, C.; Arends, I. W. C. E.; Hollmann, F. Access to Lactone Building Blocks via Horse Liver Alcohol Dehydrogenase-Catalyzed Oxidative Lactonization. *ACS Catal.* **2013**, *3*, 2436−2439.

(19) Kara, S.; Spickermann, D.; Schrittwieser, J. H.; Leggewie, C.; van Berkel, W. J. H.; Arends, I. W. C. E.; Hollmann, F. More Efficient Redox Biocatalysis by Utilizing 1,4-Butanediol as a 'Smart Cosubstrate'. *Green Chem.* **2013**, *15*, 330−335.

(20) Wachtmeister, J.; Jakoblinnert, A.; Rother, D. Stereoselective Two-Step Biocatalysis in Organic Solvent: Toward All Stereoisomers of a 1,2-Diol at High Product Concentrations. *Org. Process Res. Dev.* **2016**, *20*, 1744−1753.

(21) Kara, S.; Spickermann, D.; Weckbecker, A.; Leggewie, C.; Arends, I. W. C. E.; Hollmann, F. Bioreductions Catalyzed by an Alcohol Dehydrogenase in Non-Aqueous Media. *ChemCatChem* **2014**, *6*, 973−976.

(22) Bornadel, A.; Hatti-Kaul, R.; Hollmann, F.; Kara, S. A Bi-enzymatic Convergent Cascade for ε-1,6-Hexanediol as a 'Double-Smart Cosubstrate'. *ChemCatChem* **2015**, *7*, 2442−2445.

(23) Huang, L.; Romero, E.; Ressmann, A. K.; Rudroff, F.; Hollmann, F.; Fraaije, M. W.; Kara, S. Nicotinamide Adenine Dinucleotide-Dependent Redox-Neutral Convergent Cascade for Lactonizations with Type II Flavin-Containing Monooxygenase. *Adv. Synth. Catal.* **2017**, *359*, 2142−2148.

DOI: 10.1021/acssuschemeng.9b03879
ACS Sustainable Chem. Eng. 2019, 7, 15706−15714

(24) Huang, L.; Sayoga, G. V.; Hollmann, F.; Kara, S. Horse Liver Alcohol Dehydrogenase-Catalyzed Oxidation Lactamization of Amino Alcohols. *ACS Catal.* **2018**, *8*, 8680−8684.
(25) Zuhse, R.; Leggewie, C.; Hollmann, F.; Kara, S. Scaling-up of "smart cosubstrate" 1,4-butanediol promoted asymmetric reduction of ethyl-4,4,4-trifluoroacetoacetate in organic media. *Org. Process Res. Dev.* **2015**, *19*, 369−372.
(26) Zhou, J. Y.; Xu, G. C.; Han, R. Z.; Dong, J. J.; Zhang, W. G.; Zhang, R. Z.; Ni, Y. Carbonyl Group-Dependent High-Throughput-Screening and Enzymatic Characterization of Diaromatic KetoneR-eductase. *Catal. Sci. Technol.* **2016**, *6*, 6320−6327.
(27) Cahn, R. S.; Ingold, S. C.; Prelog, V. Specification of Molecular Chirality. *Angew. Chem., Int. Ed. Engl.* **1966**, *5*, 385−415.
(28) Xu, G. C.; Wang, Y.; Tang, M. H.; Zhou, J. Y.; Zhao, J.; Han, R. Z.; Ni, Y. Hydroclassified Combinatorial Saturation Mutagenesis: Reshaping Substrate Binding Pockets of *Kp*ADH for Enantioselective Reduction of Bulky−Bulky Ketones. *ACS Catal.* **2018**, *8*, 8336−8345.
(29) Zhou, J.; Wang, Y.; Xu, G.; Wu, L.; Han, R.; Schwaneberg, U.; Rao, Y.; Zhao, Y.-L.; Zhou, J.; Ni, Y. Structural Insight into Enantioselective Inversion of an Alcohol Dehydrogenase Reveals a "Polar Gate" in Stereorecognition of Diaryl Ketones. *J. Am. Chem. Soc.* **2018**, *140*, 12645−12654.
(30) Park, H. J.; Jung, J.; Choi, H.; Uhm, K. N.; Kim, H. K. Enantioselective Bioconversion Using *Escherichia coli* Cells Expressing *Saccharomyces cerevisiae* Reductase and *Bacillus subtilis* Glucose Dehydrogenase. *J. Microbiol. Biotechnol.* **2010**, *20*, 1300−1306.
(31) Qin, F. Y.; Qin, B.; Mori, T.; Wang, Y.; Meng, L. X.; Zhang, X.; Jia, X.; Abe, I.; You, S. Engineering of *Candida glabrata*Ketoreductase 1 for Asymmetric Reduction of alpha-Halo Ketones. *ACS Catal.* **2016**, *6*, 6135−6140.
(32) Wratten, C. C.; Cleland, W. W. Product Inhibition Studies on Yeast and Liver Alcohol Dehydrogenases. *Biochemistry* **1963**, *2*, 935−941.
(33) Hayashi, J. J.; Seto, T.; Akita, H.; Watanabe, M.; Hoshino, T.; Yoneda, K.; Ohshima, T.; Sakuraba, H. Structure-based Engineering of an Artificially Generated $NADP^+$-Dependent D-amino acid Dehydrogenase. *Appl. Environ. Microbiol.* **2017**, *83*, No. e00491−17.
(34) White, J. R.; Campbell, R. K. Recent Developments in the Pharmacological Reduction of Blood Glucose in Patients with Type 2 Diabetes. *Clin. Diabetes* **2001**, *19*, 153−159.
(35) Gao, X. Z.; Huang, F.; Feng, J. H.; Chen, X.; Zhang, H. L.; Wang, Z. X.; Wu, Q. Q.; Zhu, D. M. Engineering the meso-Diaminopimelate Dehydrogenase from *Symbiobacteriumthermophilum* by Site Saturation Mutagenesis for D-Phenylalanine Synthesis. *Appl. Environ. Microbiol.* **2013**, *79*, 5078.
(36) Makino, Y.; Negoro, S.; Urabe, I.; Okada, H. Stability-Increasing Mutants of Glucose Dehydrogenase from *Bacillus megaterium* IWG3. *J. Biol. Chem.* **1989**, *264*, 6381−6385.
(37) Filling, C.; Berndt, K. D.; Benach, J.; Knapp, S.; Prozorovski, T.; Nordling, E.; Ladenstein, R.; Jörnvall, H.; Oppermann, U. Critical Residues for Structure and Catalysis in Short-Chain Dehydrogenases/Reductases. *J. Biol. Chem.* **2002**, *277*, 25677−25684.
(38) Schlieben, N. H.; Niefind, K.; Müller, J.; Riebel, B.; Hummel, W.; Schomburg, D. Atomic Resolution Structures of *R*-Specific Alcohol Dehydrogenase from *Lactobacillus brevis* Provide the Structural Bases of its Substrate and Cosubstrate Specificity. *J. Mol. Biol.* **2005**, *349*, 801−813.

DOI: 10.1021/acssuschemeng.9b03879
ACS Sustainable Chem. Eng. 2019, 7, 15706−15714